Estimation of modal parameters of a beam under random excitation using a novel 3D continuously scanning laser Doppler vibrometer system and an extended demodulation method

K. Yuan, W.D. Zhu *

Department of Mechanical Engineering, University of Maryland, Baltimore County, 1000 Hilltop Circle, Baltimore, MD 21250, United States

ABSTRACT

A novel three-dimensional (3D) continuously scanning laser Doppler vibrometer (CSLDV) system that contains three CSLDVs and an external controller is developed to measure 3D vibration of a structure under random excitation, and a new operational modal analysis method is proposed to estimate its 3D modal parameters, including damped natural frequencies and undamped end-to-end mode shapes, by extending the conventional demodulation method. Calibration among three CSLDVs in the 3D CSLDV system based on the geometrical model of its scan mirrors is conducted to adjust their rotational angles and ensure that three laser spots can continuously and synchronously move along the same scan path on the structure. The extended demodulation method can estimate undamped mode shapes of the structure under random excitation by filtering raw response with a bandpass filter and multiplying the filtered response by sinusoidal signals with its damped natural frequencies obtained from the fast Fourier transform of raw response. Experimental investigation on one-dimensional (1D) and 3D CSLDV measurements for modal parameter estimation is conducted on a beam under white-noise excitation to validate the extended demodulation method and examine the accuracy of the 3D CSLDV system. Modal assurance criterion (MAC) values between the first four undamped mode shapes of the beam from 1D CSLDV measurement and corresponding damped mode shapes from 1D step-wise scanning measurement are larger than 95%. MAC values between the first four undamped mode shapes of the beam from 3D CSLDV measurement and corresponding damped mode shapes from 3D step-wise scanning measurement are larger than 90% in all the three directions of a specified measurement coordinate system.

© 2021 Elsevier Ltd. All rights reserved.

1. Introduction

A laser Doppler vibrometer (LDV) provides a non-contact way to measure velocity of a point on a structure based on Doppler shift in the frequency of its laser beam [1,2]. In order to automate a vibration test, a scanning laser Doppler vibrometer (SLDV) was developed by adding a pair of orthogonally mounted galvanometer mirrors to the LDV. Scan mirrors are controlled by a computer to move the laser spot to different measurement points after finishing measurement at one position. However, it usually takes a long time to obtain high spectral resolution when the surface of the structure is large and

* Corresponding author.
E-mail addresses: kyuan1@umbc.edu (K. Yuan), wzhu@umbc.edu (W.D. Zhu).

measurement points are dense [3]. An improved method is to continuously move the laser spot over the surface of the structure, which was developed as a continuously scanning laser Doppler vibrometer (CSLDV) system [3–5].

Several methods have been developed to estimate modal parameters, including natural frequencies, mode shapes, and damping ratios, of a structure under sinusoidal [6], impact [7,8] and multi-sine [9,10] excitations by processing its responses measured by the CSLDV system. Stanbridge and Ewins [6] developed two methods, which are the demodulation method and polynomial method, to obtain operational deflection shapes (ODS) of a structure under sinusoidal excitation from response measured by the CSLDV system. The demodulation method can be used to obtain ODSs of the structure by multiplying response measured by the CSLDV system by sinusoid signals with the excitation frequency and applying a low-pass filter to the multiplied response. The polynomial method can be used to obtain ODSs of the structure by processing the discrete Fourier transform of the measured response. Chen et al. [11] developed a baseline-free method by combining the demodulation and polynomial methods to identify damage in beams under sinusoidal excitation. The demodulation method was later used alone to identify damages in beams [12] and plates [13]. However, the conventional demodulation method can only be used to estimate ODSs of a structure under sinusoidal excitation. Xu et al. [14] developed a concept of free response shape that can be combined with the demodulation method to estimate modal parameters of a structure under unknown impact excitation. For a structure under unknown random excitation, an operational modal analysis (OMA) needs to be used to estimate its modal parameters. Yang and Allen [15] developed an OMA method based on the lifting method with CSLDV measurement using harmonic transfer functions and harmonic power spectra to extract natural frequencies and mode shapes of a structure under ambient excitation. Mode shapes of the structure estimated by the method are represented by sums of sinusoidal functions and spatially smooth over the scan path on the structure, which means that they cannot be used to detect damage of the structure. To estimate modal parameters and detect local anomaly of a damaged structure under random excitation, Xu et al. [16] proposed a new OMA method based on the lifting method with CSLDV measurement, which cannot easily estimate modal parameters of the structure corresponding to high natural frequencies since a high scanning frequency is necessary for the lifting method. To date, the demodulation method, which does not need a high scanning frequency, has not been used with CSLDV measurement to estimate modal parameters of a structure under random excitation.

To estimate three-dimensional (3D) modal parameters of a structure, a 3D SLDV system, which contains three SLDVs and controls three laser spots to synchronously move in a step-wise manner, has been developed to measure three perpendicular velocity components of the structure and commercialized as Polytec PSV-400-3D and PSV-500-3D. The 3D SLDV system has been applied in many areas, such as identifying fatigue cracks from in-plane and out-of-plane vibrations [17], estimating dynamic in-plane strains [18], and detecting damage in a beam by using its longitudinal vibration shapes [19]. Considering the high cost of a commercial 3D SLDV system, some investigations focused on using a single SLDV to measure 3D vibration [20,21]. Chen and Zhu [22] measured 3D vibration of a point on a beam under sinusoidal excitation by sequentially placing a single SLDV at three different positions and reported good agreement with results from a commercial Polytec PSV-500-3D. Weekes and Ewins [23] used a single CSLDV combined with a Microsoft Kinect to obtain 3D ODSs of a blade under multi-frequency excitation by sequentially placing the single CSLDV at three independent positions; the Microsoft Kinect was used to measure distances from the single CSLDV to the blade. The main challenge of using a single CSLDV for 3D ODS measurement is to ensure that the scan trajectory is the same when it is sequentially placed at three different positions. Also, using a single SLDV or CSLDV to measure 3D vibration cannot deal with transient vibration measurement.

In this study, a novel 3D CSLDV system, which contains three CSLDVs and an external controller, is developed to measure 3D vibration of a structure under random excitation, and a new OMA method is proposed to estimate its 3D modal parameters, including damped natural frequencies and undamped end-to-end mode shapes, by extending the conventional demodulation method. The proposed 3D CSLDV system differs from existing commercial 3D SLDV systems in the calibration method. Current commercial 3D SLDV systems, such as a Polytec PSV-500-3D, calibrate three laser spots by a video triangulation procedure when moving laser spots from one measurement point to the next one, which increases testing time and limits its application to continuous scanning. In the proposed 3D CSLDV system, relations between a specified measurement coordinate system (MCS) and vibrometer coordinate systems (VCSs) of three CSLDVs are calibrated through the geometrical model of its scan mirrors, and their rotational angles are adjusted to ensure that three laser spots can move along the same scan path on the structure not only continuously, but also synchronously. The proposed 3D CSLDV system is more advanced since it have both step scanning and continuous scanning manners, and can save testing time by using a pre-designed scan path. As previously mentioned, the conventional demodulation method can only process response of a structure under sinusoidal excitation and obtain its ODS corresponding to the excitation frequency. In the new OMA method, the conventional demodulation method is extended through a pre-processing procedure, in which the i-th damped natural frequency is obtained from the fast Fourier transform (FFT) of raw response of the structure under random excitation measured by the 3D CSLDV system, and a bandpass filter is used to filter raw response to allow only the identified i-th damped natural frequency of the structure to pass through it. In this way, the i-th 3D undamped mode shape of the structure can be obtained by multiplying the filtered response by sinusoidal signals with the i-th damped natural frequency of the structure and applying a low-pass filter to the multiplied response. By extending the conventional demodulation method, both damped natural frequencies and undamped mode shapes of the structure under random excitation can be obtained in one modal testing, which means that the proposed OMA method is more effective. With more vibration information than one-dimensional (1D) mode shapes of a structure, estimated 3D mode shapes of the structure can be used to detect its damage in some future study.

Experimental investigation on 1D and 3D CSLDV measurements for natural frequency and mode shape estimation was conducted on a beam under white-noise excitation to validate the extended demodulation method and examine the accuracy of the 3D CSLDV system. Damped natural frequencies and mode shapes of the beam obtained from a Polytec PSV-500 in its 1D and 3D step-wise scanning manners were used as references for comparison purposes. With a sampling frequency of 125 kHz, errors between the first four damped natural frequencies of the beam from 1D CSLDV measurements and those from step-wise scanning measurement are less than 1.3%. Modal assurance criterion (MAC) values between the first four undamped mode shapes of the beam from above 1D CSLDV measurements and corresponding damped mode shapes from 1D step-wise scanning measurement are larger than 95%, which validates the effectiveness of the extended demodulation method in estimating undamped mode shapes of a structure under random excitation. MAC values between the first four undamped mode shapes of the beam from 3D CSLDV measurement and corresponding damped mode shapes from 3D step-wise scanning measurement are larger than 90% in all the three directions of the specified MCS, indicating that the extended demodulation method can be used to estimate 3D mode shapes of a structure under random excitation and the 3D CSLDV system has essentially the same level of accuracy as that of 3D step-wise scanning measurement in obtaining 3D vibration of the structure under random excitation. However, the 3D CSLDV system can scan much more measurement points in much less time and provide smoother mode shapes than those from the 3D step-wise scanning manner of a Polytec PSV-500-3D. Note that the first four undamped mode shapes of the beam are bending mode shapes whose in-plane components are not significant, since it was excited along the transverse direction in this work. The potential application of the 3D CSLDV system on identifying longitudinal mode shapes would be investigated in the future by using multiple excitation sources along different directions.

Novelties of this work are summarized as follows. First, a novel 3D CSLDV system that contains three CSLDVs is developed to measure 3D vibration of a structure by continuously and synchronously moving three laser spots along the same scan path on its surface. Second, a new OMA method for estimating damped natural frequencies and undamped end-to-end mode shapes of a structure under random excitation with CSLDV measurement is proposed by extending the conventional demodulation method. Third, the extended demodulation method is used with the 3D CSLDV system to estimate 3D undamped mode shapes of a structure under random excitation.

The remaining part of this paper is organized as follows. The geometrical model of the 3D CSLDV system and its calibration method are presented in Section 2.1, and the extended demodulation method to estimate modal parameters of a structure under random excitation with CSLDV measurement is presented in Section 2.2. Experimental setup of this study and details about calibration among three CSLDVs in the 3D CSLDV system are presented in Section 3.1. Experimental results of 1D and 3D mode shape estimation of a beam under white-noise excitation for validating the extended demodulation method and examining the accuracy of the 3D CSLDV system are presented in Sections 3.2 and 3.3, respectively. Conclusions of this work are presented in Section 4.

2. Methodology

2.1. Description of the 3D CSLDV system

The 3D CSLDV system in this study consists of three CSLDVs, which are referred to as Top, Left, and Right CSLDVs based on their positions during measurement, and an external controller, as shown in Fig. 1. Scan mirrors in each CSLDV are driven by the external controller, which directs three laser spots to continuously and synchronously move along the same prescribed scan path.

2.1.1. Geometrical model of a CSLDV

In order to measure 3D vibration of a structure, a MCS and a VCS need to be first defined [22]. Two orthogonal scan mirrors in a CSLDV are referred to as X and Y mirrors in this work. As shown in Fig. 2, the *o-xyz* coordinate system is the MCS and the *o′-x′y′z′* coordinate system is the VCS of the CSLDV. In this study, a Polytec PSV-A-450 reference object, which has some known accurate coordinates, is used as the MCS; so the MCS can be moved to any desirable position depending on how one
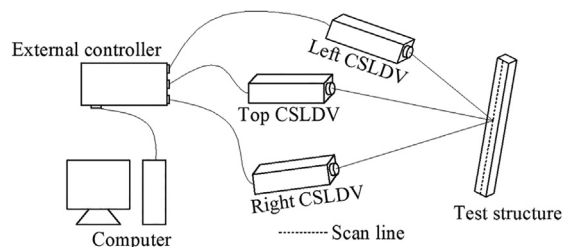

Fig. 1. Schematic of the 3D CSLDV system where an external controller directs laser spots of three CSLDVs to continuously and synchronously move along the same prescribed scan path.
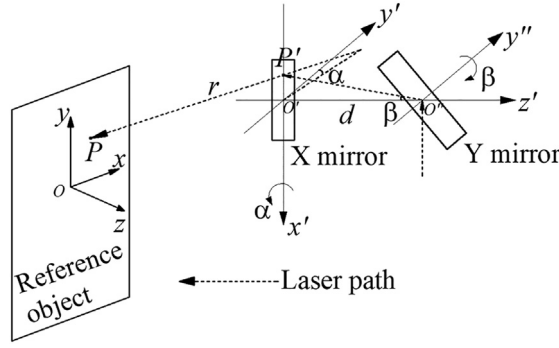
Fig. 2. Geometrical model of X and Y mirrors of the CSLDV, in which the reference object is used as the MCS to provide points with known coordinates.

would like to set up coordinates in measurement. Coordinates of a measurement point P in the MCS are expressed as $\mathbf{P}_{MCS} = [x, y, z]^T$. The VCS of the CSLDV is built on its two scan mirrors and describes its position during measurement. One can see from Fig. 2 that the origin of the VCS o' is fixed at the center of the X mirror and o'' is fixed at the center of the Y mirror; so the X mirror can rotate about the x' axis, and the Y mirror can rotate about the y'' axis that is parallel to the y' axis. Variables α and β that can be controlled by inputting voltages to X and Y mirrors through the external controller are rotational angles of X and Y mirrors from their initial positions, respectively. The distance between centers of the two scan mirrors d is a known parameter for the CSLDV, which is 29.2 mm in this study. Based on the geometrical model of the CSLDV in Fig. 2, coordinates of the measurement point P in the VCS can be expressed as

$$\mathbf{P}_{VCS} = [-d\tan(\beta) - r\sin(\beta), -r\cos(\alpha)\cos(\beta), -r\sin(\alpha)\cos(\beta)]^T \tag{1}$$

where r is the distance from the measurement point P to the incident point of the laser path on the X mirror P'. The relation between $\mathbf{P}_{MCS}$ and $\mathbf{P}_{VCS}$ can then be written as

$$\mathbf{P}_{MCS} = \mathbf{T} + \mathbf{R}\mathbf{P}_{VCS} = \begin{bmatrix} x_{o'} \\ y_{o'} \\ z_{o'} \end{bmatrix} + \begin{bmatrix} \cos(x,x') & \cos(x,y') & \cos(x,z') \\ \cos(y,x') & \cos(y,y') & \cos(y,z') \\ \cos(z,x') & \cos(z,y') & \cos(z,z') \end{bmatrix} \begin{bmatrix} -d\tan(\beta) - r\sin(\beta) \\ -r\cos(\alpha)\cos(\beta) \\ -r\sin(\alpha)\cos(\beta) \end{bmatrix} \tag{2}$$

where $\mathbf{T} = [x_{o'}, y_{o'}, z_{o'}]^T$ is the translation vector that denotes coordinates of the origin o' in the MCS, and $\mathbf{R}$ is the direction cosine matrix from the MCS to the VCS. In order to determine $\mathbf{R}$ and $\mathbf{T}$ matrices, coordinates of at least four points in the MCS and VCS need to be known. In Eq. (2), coordinates of points in the MCS can be obtained by inputting voltages to scan mirrors to accurately direct laser spots to points provided by the reference object, and rotational angles of scan mirrors are determined by voltages inputted to them; so the distance r is the only unknown variable that needs to be calculated.

The distance between two arbitrary spatial points P^m and P^n is an absolute value that remains the same in different coordinate systems, which can be expressed as

$$|\mathbf{P}_{MCS}^m - \mathbf{P}_{MCS}^n| = |\mathbf{P}_{VCS}^m - \mathbf{P}_{VCS}^n| \tag{3}$$

Assuming that the total number of spatial points used to determine $\mathbf{R}$ and $\mathbf{T}$ is H; m is from 1 to $H-1$ and n is from $m+1$ to H. Since $H \geqslant 4$ in this study, $H(H-1)/2$ equations like Eq. (3) can be formed to construct an over-determined nonlinear problem. Exact values of r for all the H points can be calculated through the nonlinear least squares method, in which roughly measured distances from the X mirror to the point P^m can be inputted as initial values of r. With calculated coordinates of H points in the MCS and VCS, $\mathbf{R}$ and $\mathbf{T}$ can be determined by solving an optimization problem [22,24]:

$$F(\mathbf{T}, \mathbf{R}) = \delta = \min \sum_{m=1}^{H} |\mathbf{P}_{MCS}^m - (\mathbf{T} + \mathbf{R}\mathbf{P}_{VCS}^m)| \tag{4}$$

In this study, three pairs of matrices of $\mathbf{R}$ and $\mathbf{T}$ can be calculated for three CSLDVs.

2.1.2. Continuously and synchronously scanning relation among three CSLDVs

Depending on the geometry of the test structure, various scan paths, such as line scan for a beam-like structure [11], zig-zag scan for a plate-like structure [13], and Lissajous trajectory scan for a geometrically-complex surface [23], can be defined by inputting corresponding voltages to scan mirrors in a CSLDV. Rotational angles of scan mirrors in the Top CSLDV to direct the laser spot to a point P^k on the scan path can be obtained when it is placed at a desired position during measurement. The variable r_{Top}^k in Eq. (1) for the Top CSLDV can be calculated by an iteration method that is based on calculation of the length of a median of a triangle. As shown in Fig. 3, the median AD of a triangle ABC can be calculated using Apollonius' theorem [25]:
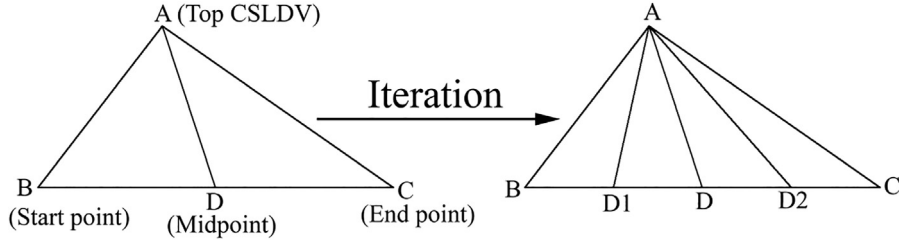
Fig. 3. Iteration method based on calculation of the length of the median AD of a triangle ABC, in which the Top CSLDV and start and end points of the scan path are placed at three vertices of ABC.

$$AD = \sqrt{\frac{1}{2}AB^2 + \frac{1}{2}AC^2 - \frac{1}{4}BC^2} \qquad (5)$$

where AB, AC, and BC are three sides of the triangle ABC. In this study, the Top CSLDV and start and end points of the scan path are placed at three vertices of ABC. Substituting r_{Top}^B and r_{Top}^C, which are lengths of two sides of ABC and can be accurately measured by the geometrical unit in the Top CSLDV, into Eq. (1), coordinates of points B and C in the VCS of the Top CSLDV, $\mathbf{P}_{VCS(Top)}^B$ and $\mathbf{P}_{VCS(Top)}^C$, can be determined; so the length of the third side of ABC is equal to the norm of the spatial vector **BC**. Therefore, the initial value of the median AD can be calculated by Eq. (5), and values of r_{Top}^k of all the points on the scan path for the Top CSLDV can be obtained by iterating and repeating calculation of medians of ABC, as shown in Fig. 3.

Since the position of the Top CSLDV with respect to the MCS has been obtained by the method described in Section 2.1.1, coordinates of the point P^k on the scan path in the MCS can be obtained by

$$\mathbf{P}_{MCS}^k = \mathbf{T}_{Top} + \mathbf{R}_{Top}\mathbf{P}_{VCS(Top)}^k \qquad (6)$$

where $\mathbf{T}_{Top}$ and $\mathbf{R}_{Top}$ are the translation vector and direction cosine matrix of the Top CSLDV with respect to the MCS, respectively. Since coordinates of the point P^k are constant in the MCS for three CSLDVs, in order to let laser spots from Left and Right CSLDVs directed to the same point P^k, positional relations among three CSLDVs for the point P^k are established by

$$\mathbf{T}_{Top} + \mathbf{R}_{Top}\mathbf{P}_{VCS(Top)}^k = \mathbf{T}_{Left} + \mathbf{R}_{Left}\mathbf{P}_{VCS(Left)}^k = \mathbf{T}_{Right} + \mathbf{R}_{Right}\mathbf{P}_{VCS(Right)}^k \qquad (7)$$

where $\mathbf{T}_{Left}$ and $\mathbf{R}_{Left}$ are the translation vector and direction cosine matrix of the Left CSLDV with respect to the MCS, respectively, and $\mathbf{T}_{Right}$ and $\mathbf{R}_{Right}$ are the translation vector and direction cosine matrix of the Right CSLDV with respect to the MCS, respectively. Hence, coordinates of the point P^k in VCSs of Left and Right CSLDVs can be obtained by

$$\mathbf{P}_{VCS(Left)}^k = \mathbf{R}_{Left}^{-1}\left[\left(\mathbf{T}_{Top} - \mathbf{T}_{Left}\right) + \mathbf{R}_{Top}\mathbf{P}_{VCS(Top)}^k\right] \qquad (8)$$

$$\mathbf{P}_{VCS(Right)}^k = \mathbf{R}_{Right}^{-1}\left[\left(\mathbf{T}_{Top} - \mathbf{T}_{Right}\right) + \mathbf{R}_{Top}\mathbf{P}_{VCS(Top)}^k\right] \qquad (9)$$

respectively. Furthermore, rotational angles of X and Y mirrors of Left and Right CSLDVs for the point P^k can be obtained by

$$\alpha_{Left}^k = \arctan\left(z_{VCS(Left)}^k/z_{VCS(Left)}^k\right)$$
$$\beta_{Left}^k = \arctan\left(x_{VCS(Left)}^k/\left(y_{VCS(Left)}^k/\cos\left(\alpha_{Left}^k\right) - d\right)\right) \qquad (10)$$

and

$$\alpha_{Right}^k = \arctan\left(z_{VCS(Right)}^k/z_{VCS(Right)}^k\right)$$
$$\beta_{Right}^k = \arctan\left(x_{VCS(Right)}^k/\left(y_{VCS(Right)}^k/\cos\left(\alpha_{Right}^k\right) - d\right)\right) \qquad (11)$$

respectively.

With the proposed methodology described above, three laser spots from three CSLDVs can continuously and synchronously move along the same scan path by inputting corresponding rotational angles to their scan mirrors. Vibration components of the point P^k in x, y, and z directions of the MCS can then be obtained by

$$\left[V_x^k, V_y^k, V_z^k\right]^T = \left[\left[\mathbf{R}_{Top}\mathbf{e}_{Top}^k, \mathbf{R}_{Left}\mathbf{e}_{Left}^k, \mathbf{R}_{Right}\mathbf{e}_{Right}^k\right]^T\right]^{-1}\left[V_{Top}^k, V_{Left}^k, V_{Right}^k\right]^T \qquad (12)$$

where $\mathbf{e}_X^k = \left[\sin(\beta_X^k), \cos(\alpha_X^k)\cos(\beta_X^k), \sin(\alpha_X^k)\cos(\beta_X^k)\right]^T$, in which the subscript X denotes Top, Left, or Right, is the unit vector in the laser beam direction in the VCS of each CSLDV when the laser spot is directed to the point P^k. The process described by Eq. (12) can be repeated for each point on the prescribed scan path. Finally, 3D vibration of the structure in the MCS can be obtained by the 3D CSLDV system.

2.2. Extended demodulation method for CSLDV measurement with random excitation

Response of a linear, time-invariant, viscously damped structure under external excitation can be obtained by solving its governing partial differential equation [26]

$$M\left[\frac{\partial^2 u(\mathbf{x},t)}{\partial t^2}\right] + C\left[\frac{\partial u(\mathbf{x},t)}{\partial t}\right] + K[u(\mathbf{x},t)] = f(\mathbf{x},t) \tag{13}$$

with known boundary conditions, where $\mathbf{x}$ denotes the spatial position of a point on the structure, t is time, u is response of the structure, $M(\cdot)$, $C(\cdot)$, and $K(\cdot)$ are mass, damping, and stiffness operators, respectively, and f is the excitation force density.

By applying the expansion theorem, a solution of Eq. (13) can be expressed as

$$u(\mathbf{x},t) = \sum_{i=1}^{\infty} \phi_i(\mathbf{x})q_i(t) \tag{14}$$

where ϕ_i and q_i are the i-th mass-normalized eigenfunction of the associated undamped structure and corresponding generalized coordinate, respectively. By assuming that the associated undamped structure is self-adjoint, ϕ_i satisfies the following orthonormality relations:

$$\int_D \phi_j(\mathbf{x})M[\phi_i(\mathbf{x})]d\mathbf{x} = \delta_{ij} \tag{15}$$

$$\int_D \phi_j(\mathbf{x})K[\phi_i(\mathbf{x})]d\mathbf{x} = \omega_i^2\delta_{ij} \tag{16}$$

where D is the spatial domain of $\mathbf{x}$, ω_i is the i-th undamped natural frequency of the structure, and δ_{ij} is Kronecker delta that satisfies

$$\delta_{ij} = \begin{cases} 0 & i \neq j \\ 1 & i = j \end{cases} \tag{17}$$

Assuming that the structure is classically damped [27], one has

$$\int_D \phi_j(\mathbf{x})C[\phi_i(\mathbf{x})]d\mathbf{x} = c_i\delta_{ij} \tag{18}$$

Substituting Eq. (14) into Eq. (13), multiplying the resulting equation by $\phi_j(\mathbf{x})$, integrating the resulting equation in the spatial domain D, and using Eqs. (15), (16), and (18) in the resulting equation yield

$$\ddot{q}_i(t) + 2\zeta_i\omega_i\dot{q}_i(t) + \omega_i^2 q_i(t) = \int_D \phi_i(\mathbf{x})f(\mathbf{x},t)d\mathbf{x} \tag{19}$$

where an overdot denotes time differentiation, and $\zeta_i = c_i/(2\omega_i)$ is the i-th modal damping ratio of the structure that is less than 1 if all its modes are assumed to be underdamped. By assuming that initial conditions of the structure are zero, the solution of Eq. (19) can be expressed as

$$q_i(t) = \int_0^t \int_D \phi_i(\mathbf{x})f(\mathbf{x},t-\tau)g_i(\tau)d\mathbf{x}d\tau \tag{20}$$

where

$$g_i(t) = \frac{1}{\omega_{d,i}}e^{-\zeta_i\omega_i t}\sin(\omega_{d,i}t) \tag{21}$$

is the unit impulse response function corresponding to the i-th mode of the structure, in which $\omega_{d,i} = \omega_i\sqrt{1-\zeta_i^2}$ is the i-th damped natural frequency of the structure. If the external excitation $f(\mathbf{x},t)$ is a random concentrated force $f_p(t)$ applied at the point $\mathbf{x}_p$ on the structure, one has

$$f(\mathbf{x},t) = \delta(\mathbf{x}-\mathbf{x}_p)f_p(t) \tag{22}$$

where δ is Dirac delta function. By substituting Eqs. (20)–(22) into Eq. (14), response u becomes

$$u(\mathbf{x}, t) = \sum_{i=1}^{\infty} \phi_i(\mathbf{x})\phi_i(\mathbf{x}_p) \int_0^t \frac{1}{\omega_{d,i}} f_p(t - \tau) e^{-\zeta_i \omega_i \tau} \sin(\omega_{d,i} \tau) \mathrm{d}\tau \qquad (23)$$

When a 1D or 3D CSLDV system is used to continuously and periodically scan the structure along a scan path **s** to measure its response, it registers discrete measurements of u with a finite sampling frequency f_{sa} and assigns N measurement points along **s**, where N is determined by the scanning frequency f_{sc} and sampling frequency f_{sa} of the CSLDV system:

$$N = \frac{f_{sa}}{2f_{sc}} \qquad (24)$$

Applying integration by parts to Eq. (23) yields

$$\begin{aligned} u(\mathbf{x}, t) = \sum_{i=1}^{N} \phi_i(\mathbf{x})\phi_i(\mathbf{x}_p) \{ &-\frac{e^{-\zeta \omega_i t} f_p(0)}{\omega_{d,i} \omega_i^2} \left[\zeta \omega_i \sin(\omega_{d,i} t) + \omega_{d,i} \cos(\omega_{d,i} t) \right] \\ &+ \frac{f_p(t)}{\omega_i^2} + \int_0^t \frac{e^{-\zeta \omega_i t} f_p'(t-\tau)}{\omega_{d,i} \omega_i^2} \left[\zeta \omega_i \sin(\omega_{d,i} t) + \omega_{d,i} \cos(\omega_{d,i} t) \right] \mathrm{d}\tau \}. \end{aligned} \qquad (25)$$

Eq. (25) can then be written as

$$u(\mathbf{x}, t) = \sum_{i=1}^{N} \phi_i(\mathbf{x})\phi_i(\mathbf{x}_p) \left[A_i(t)\cos(\omega_{d,i} t) + B_i(t)\sin(\omega_{d,i} t) + C_i(t) \right] \qquad (26)$$

where $A_i(t)$, $B_i(t)$, and $C_i(t)$ are arbitrary functions of time related to the concentrated force $f_p(t)$ that is assumed to be white-noise excitation in this study. By applying a bandpass filter that allows only the i-th damped natural frequency of the structure $\omega_{d,i}$ to pass through it, response u in Eq. (26) can be expressed as

$$u_i(\mathbf{x}, t) = \Phi_i(\mathbf{x})\cos(\omega_{d,i} t - \varphi) = \Phi_{I,i}(\mathbf{x})\cos(\omega_{d,i} t) + \Phi_{Q,i}(\mathbf{x})\sin(\omega_{d,i} t) \qquad (27)$$

where $u_i(\mathbf{x}, t)$ is the filtered response of $u(\mathbf{x}, t)$, $\Phi_i(\mathbf{x})$ are responses at measurement points along the scan path that have two components, which are the in-phase component $\Phi_{I,i}(\mathbf{x})$ and quadrature component $\Phi_{Q,i}(\mathbf{x})$, and φ is a phase variable.

With bandpass filtering and the filtered response obtained from Eq. (27), the conventional demodulation method in [6,11] is extended to obtain in-phase and quadrature components of $\Phi_i(\mathbf{x})$. To this end, multiplying $u_i(\mathbf{x}, t)$ in Eq. (27) by $\cos(\omega_{d,i} t)$ and $\sin(\omega_{d,i} t)$ yields

$$\begin{aligned} u_i(\mathbf{x}, t)\cos(\omega_{d,i} t) &= \Phi_{I,i}(\mathbf{x})\cos^2(\omega_{d,i} t) + \Phi_{Q,i}(\mathbf{x})\sin(\omega_{d,i} t)\cos(\omega_{d,i} t) \\ &= \tfrac{1}{2}\Phi_{I,i}(\mathbf{x}) + \tfrac{1}{2}\Phi_{I,i}(\mathbf{x})\cos(2\omega_{d,i} t) + \tfrac{1}{2}\Phi_{Q,i}(\mathbf{x})\sin(2\omega_{d,i} t), \end{aligned} \qquad (28)$$

$$\begin{aligned} u_i(\mathbf{x}, t)\sin(\omega_{d,i} t) &= \Phi_{I,i}(\mathbf{x})\sin(\omega_{d,i} t)\cos(\omega_{d,i} t) + \Phi_{Q,i}(\mathbf{x})\sin^2(\omega_{d,i} t) \\ &= \tfrac{1}{2}\Phi_{Q,i}(\mathbf{x}) + \tfrac{1}{2}\Phi_{I,i}(\mathbf{x})\sin(2\omega_{d,i} t) - \tfrac{1}{2}\Phi_{Q,i}(\mathbf{x})\cos(2\omega_{d,i} t), \end{aligned} \qquad (29)$$

respectively. A low-pass filter can then be used to eliminate $\sin(2\omega_{d,i} t)$ and $\cos(2\omega_{d,i} t)$ terms in Eqs. (28) and (29), and corresponding results can be multiplied by a scale factor of two to obtain $\Phi_{I,i}(\mathbf{x})$ and $\Phi_{Q,i}(\mathbf{x})$. The i-th undamped end-to-end mode shape of the structure under random excitation can be finally obtained.

3. Experimental investigation

3.1. Experimental setup

A Polytec PSV-500-3D with three SLDVs was used to build the 3D CSLDV system in this work, and vibrations of a beam under random excitation measured in its 1D and 3D step-wise scanning manners were used as references for comparison purposes to validate the extended demodulation method and examine the accuracy of the 3D CSLDV system developed in this study. Since the continuously scanning manner is not directly provided by the Polytec PSV-500-3D, an external controller unit needs to be connected to the interface connector in each SLDV through BNC cables to extend SLDVs to CSLDVs. As shown in Fig. 4(a), a dSPACE MicroLabBox and the ControlDesk software were used as the external controller to generate a series of signals to control a total number of six scan mirrors to continuously rotate in the configured 3D CSLDV system in this work. Also, the external controller in Fig. 4(a) can be removed from the 3D CSLDV system to obtain the original Polytec PSV-500-3D and conduct step-wise scanning measurement. In the 3D CSLDV measurement, three CSLDVs should be placed at proper locations. The longitudinal axis of the scan head of the Top CSLDV needs to be perpendicular to the scan surface of the beam. Left and Right CSLDVs can be placed at arbitrary locations as long as they are not too close to the Top CSLDV and their laser spots can cover the complete area to be scanned in the input voltage range. A range of 30° to 60° is recommended for the angle between the longitudinal axis of the scan head of the Left or Right CSLDV and the normal direction of the scan surface.
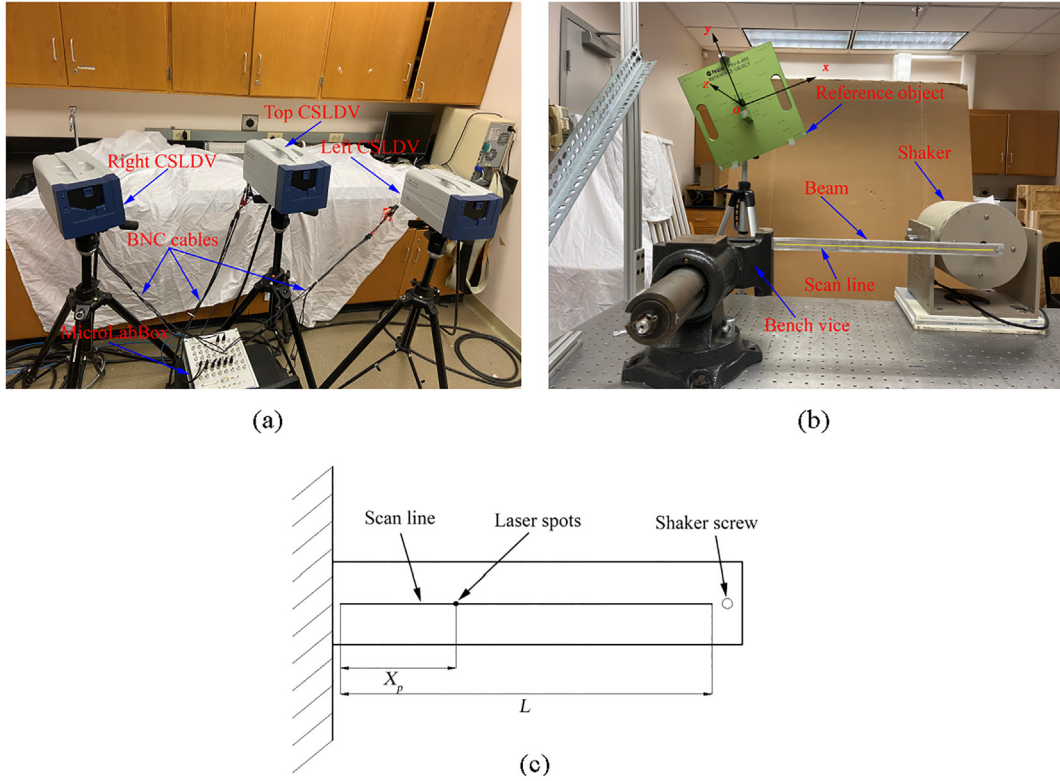
Fig. 4. (a) Components of the 3D CSLDV system where a dSPACE MicroLabBox was used as the external controller and three SLDVs in the Polytec PSV-500-3D were extended to three CSLDVs through their interface connectors; (b) the test beam that was clamped by a bench vice at its left end and screwed to a shaker at its right end; and (c) the distance between laser spots and the start point of the scan line X_p, and the length of the scan line L, which were used to locate laser spots by a normalized length scale X_p/L.

A scan line from one end of the test beam to its other end was designed, as shown in Fig. 4(b). A bench vice was used to clamp the left end of the beam to simulate a fixed boundary, and a MB Dynamics MODAL-50 shaker was screwed to its right end to excite it by white-noise excitation. A strip of reflective tape was attached to the surface of the beam to enhance the signal-to-noise ratio (SNR) of measurement. A total number of six points with known coordinates in the PSV-A-450 reference object were selected to calculate translation vectors **T** and direction cosine matrices **R** of three CSLDVs by following the method described in Section 2.1. Effects of the number and locations of reference points on calibration results were investigated in Ref. [22], which shows that translation vectors and direction cosine matrices are not significantly affected when the number of reference points changes from four to twelve. In this work, six reference points including four corner points and one reference point on either of two poles are selected to represent the basic shape of the PSV-A-450 reference object. The coordinate system o-xyz based on the reference object shown in Fig. 4(b) was used as the MCS, whose z axis almost aligns with the out-of-plane direction of the beam in this study. One can see from Fig. 4(c) that the position of laser spots can be located by a normalized length scale X_p/L, where X_p is the distance between laser spots and the start point of the scan line that is close to the fixed boundary of the beam, and L is the length of the scan line. A complete scan period is defined as sweeping laser spots from $X_p/L = 0$ to $X_p/L = 1$ and back again. In step-wise scanning measurement of the Polytec PSV-500-3D, a total number of 101 measurement points were created along the above scan line to measure 1D and 3D vibrations of the beam and estimate its modal parameters, including damped natural frequencies and mode shapes, as references for comparison purposes in this study. A detailed description for calculating rotational angles of scan mirrors in Left and Right CSLDVs and calibrating the 3D CSLDV system is provided below:

1 Control scan mirrors in three CSLDVs to successively direct their laser spots to six reference points on the PSV-A-450 reference object, record their coordinates in the MCS and corresponding rotational angles, and use Eqs. (1)–(4) to obtain translation vectors and direction cosine matrices of three CSLDVs.
2 Design a scan line on the test beam, record rotational angles of scan mirrors in the Top CSLDV for start and end points on the scan line, measure distances from the Top CSLDV to start and end points, and use the iteration method in Section 2.1.2 to obtain r^k of each point on the scan line.
3 Use Eqs. (8)–(11) to calculate rotational angles of scan mirrors corresponding to Left and Right CSLDVs.

4 Feed signals corresponding to rotational angles calculated in above steps to three CSLDVs, and visually examine if three laser spots can continuously and synchronously move along the same scan line.

It is noted that the third step in the above description is significant to achieve the aim of synchronous scanning. It is easy to obtain input signals of scan mirrors for measurement with a single CSLDV by linearly dividing values between signal peaks corresponding to start and end points on the scan line. For the 3D CSLDV system in this study, however, the approach of linear division can generate signals to control three laser spots to move along the same scan line, but not synchronously, since it is difficult to keep all the laser beams from three CSLDVs to be absolutely perpendicular to the test beam and any slight angle changes would lead to asynchronous scanning. Signals inputted to six scan mirrors with a scanning frequency of $f_{sc} = 1$ Hz are selected to show differences between actual signals that cause three laser spots to synchronously move along the same scan line and linear signals that are directly obtained by the linear division approach. Signals inputted to scan mirrors for a complete scanning period in a duration of 1 s are shown in Fig. 5, where Fig. 5(a) and (b) are X and Y mirror signals for the Top CSLDV, Fig. 5(c) and (d) are corresponding signals for the Left CSLDV, and Fig. 5(e) and (f) are corresponding signals for the Right CSLDV. One can see from Fig. 5(a) and (b) that actual signals to the Top CSLDV are linear since they are used as references to calculate signals to the other two CSLDVs. It is obvious that actual signals to Left and Right CSLDVs, which are calibrated by the proposed method in this work, have slight curvatures compared to linear signals, indicating that there are differences between actual signals and linear signals and the proposed calibration method is necessary. To further check the effect of calibration on synchronous scanning, distances between the laser spot from the Top CSLDV and those from Left and Right CSLDVs, which are zero in theory, are calculated at each position along the scan path. Standard deviations of all the distances are 0.11 mm and 0.24 mm for Left and Right CSLDVs, respectively. They have the same order of magnitude as the diameter of the laser spot, which is 0.15 mm, and slight errors are induced by visual observation during calibration.

3.2. Estimated damped natural frequencies and 1D undamped end-to-end mode shapes of the test beam from CSLDV measurements

In order to validate the extended demodulation method proposed in this work, 1D transverse vibration of the test beam under white-noise excitation was measured using one of the three CSLDVs mentioned in Section 3.1, and its first four 1D undamped end-to-end mode shapes were estimated by the extended demodulation method. The procedure for obtaining the second undamped end-to-end mode shape of the beam in 1D CSLDV measurement with $f_{sc} = 1$ Hz and $f_{sa} = 125$ kHz is shown in Fig. 6 as an example to demonstrate main steps of the extended demodulation method. As shown in Fig. 6(a), the first step is applying the FFT to raw response of the beam to obtain its i-th damped natural frequency $\omega_{d,i}$. One can see that the second damped natural frequency of the beam, which is marked by a dashed line, is 356.3 Hz for this measurement. The second step is creating a bandpass filter to allow only the damped natural frequency identified in the first step to pass through it. In this case, the passband of the filter was set from 356 to 357 Hz, which contains only the identified frequency of 356.3 Hz. The filtered response is shown in Fig. 6(b), where the dashed line denotes feedback signals of the X mirror that are synchronous with response of the beam, whose FFT is shown in Fig. 6(c), where one can see that its peak value is exactly at the frequency 356.3 Hz. The third step is selecting a time interval $[T_1, T_2]$ in mirror signals, in which mirror signals start at their minimum value and end at their maximum value, as shown in Fig. 6(b); so response in the time interval is an end-to-end response from $X_p/L = 0$ to $X_p/L = 1$. The fourth step is multiplying the filtered response in the second step in the time interval selected in the third step by sinusoidal signals $\cos(\omega_{d,i}t)$ and $\sin(\omega_{d,i}t)$, where $\omega_{d,i}$ is the damped natural frequency identified in the first step, and subsequently applying a low-pass filter to the multiplied response to eliminate $\sin(2\omega_{d,i}t)$ and $\cos(2\omega_{d,i}t)$ terms in Eqs. (28) and (29) and obtain the final undamped end-to-end mode shape of the beam. The second normalized undamped end-to-end mode shape of the beam estimated by above steps is shown in Fig. 6(d). Note that a mode shape of the beam is normalized in this work by dividing its values by its maximum absolute value. One can see from Fig. 6(d) that the amplitude of the estimated mode shape of the beam at the position $X_p/L = 0$ is very small but not zero, since the start point of the scan line is close to, but not exactly at, the fixed boundary of the beam, which can be seen in Fig. 4.

The first four normalized 1D undamped end-to-end mode shapes of the beam under white-noise excitation from 1D CSLDV measurement are compared to its damped mode shapes from 1D step-wise scanning measurement to validate the extended demodulation method. Note that damping ratios of the beam in this study are small and have little effect on its mode shapes. MAC values are used to show correlation between undamped mode shapes from 1D CSLDV measurement and corresponding damped mode shapes from 1D step-wise scanning measurement; correlation is high when a MAC value is close to 1 and low when it is close to 0 [28]. As mentioned in Section 3.1, a total number of 101 measurement points were created along the scan line in step-wise scanning measurement, and the number of measurement points in CSLDV measurement N is determined by its sampling and scanning frequencies in Eq. (24).

Test conditions, including numbers of measurement points and test durations, of 1D CSLDV measurements with the same scanning frequency of 1 Hz and different sampling frequencies of 125, 50, and 25 kHz, and those of 1D step-wise scanning measurement are shown in Table 1; corresponding test conditions of 1D CSLDV measurements with the same sampling frequency of 125 kHz and different scanning frequencies of 1 and 0.5 Hz are shown in Table 2. One can see from Tables 1 and 2 that 1D CSLDV measurements with the same scanning frequency of 1 Hz and different sampling frequencies of 125, 50, and 25 kHz have 62,500, 25,000, and 12,500 measurement points, respectively, 1D CSLDV measurement with a scanning frequency of 0.5 Hz and a sampling frequency of 125 kHz has 125,000 measurement points, and above 1D CSLDV measurements
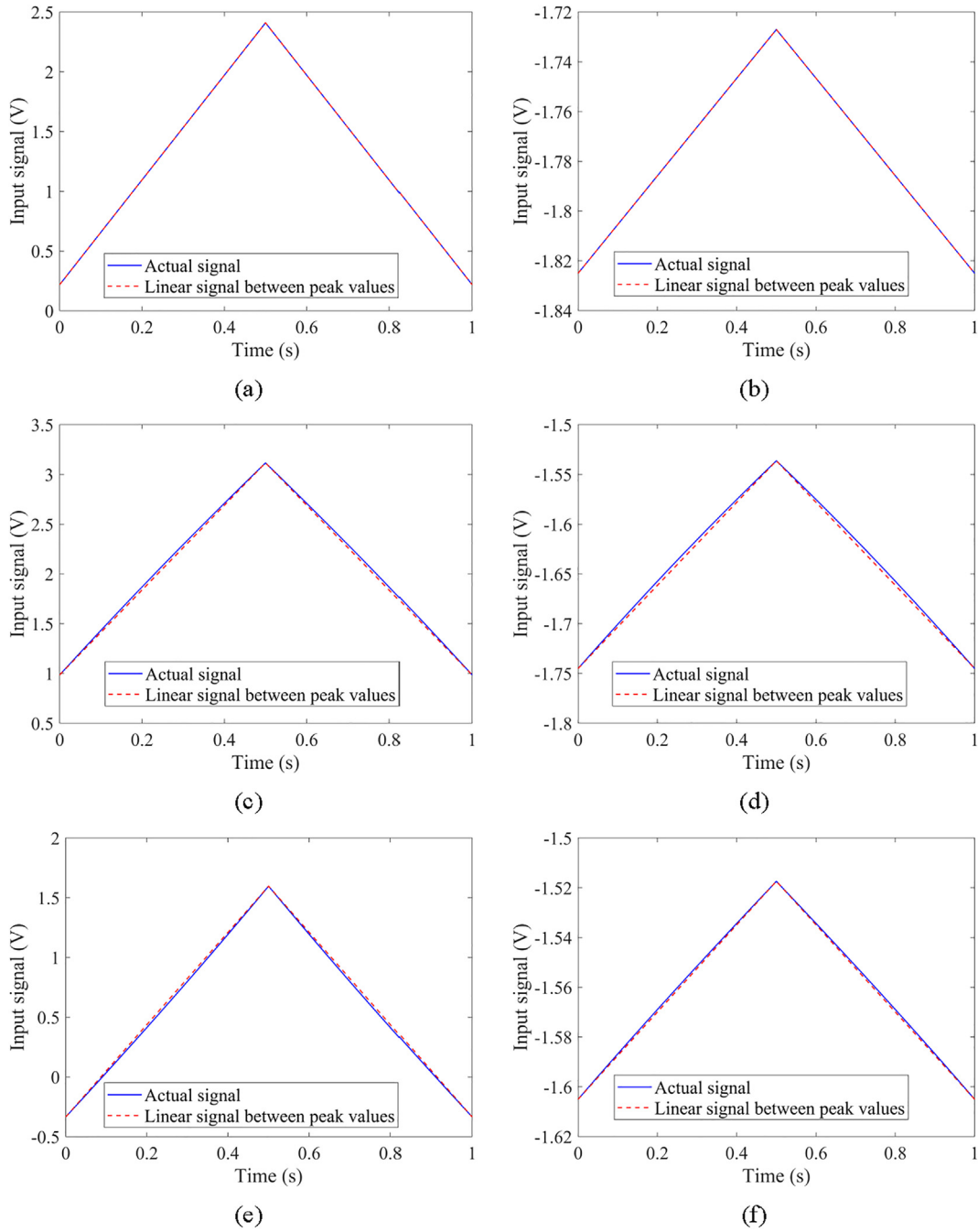
Fig. 5. Differences between actual signals that cause three laser spots to synchronously move along the same scan line and linear signals that are directly obtained by the linear division approach for (a) the X mirror in the Top CSLDV, (b) the Y mirror in the Top CSLDV, (c) the X mirror in the Left CSLDV, (d) the Y mirror in the Left CSLDV, (e) the X mirror in the Right CSLDV, and (f) the Y mirror in the Right CSLDV.

all have the same test duration of 50 s; 1D step-wise scanning measurement has 101 measurement points and a test duration of 776 s. It can be concluded that 1D CSLDV measurements have much more measurement points than 1D step-wise scanning measurement but take much less time in testing. One can also see from Tables 1 and 2 the first four damped natural frequencies of the beam from 1D CSLDV measurements and those from 1D step-wise scanning measurement, and MAC values between the first four undamped mode shapes of the beam from 1D CSLDV measurements and corresponding damped mode shapes from 1D step-wise scanning measurement. The first four normalized undamped end-to-end mode shapes of the
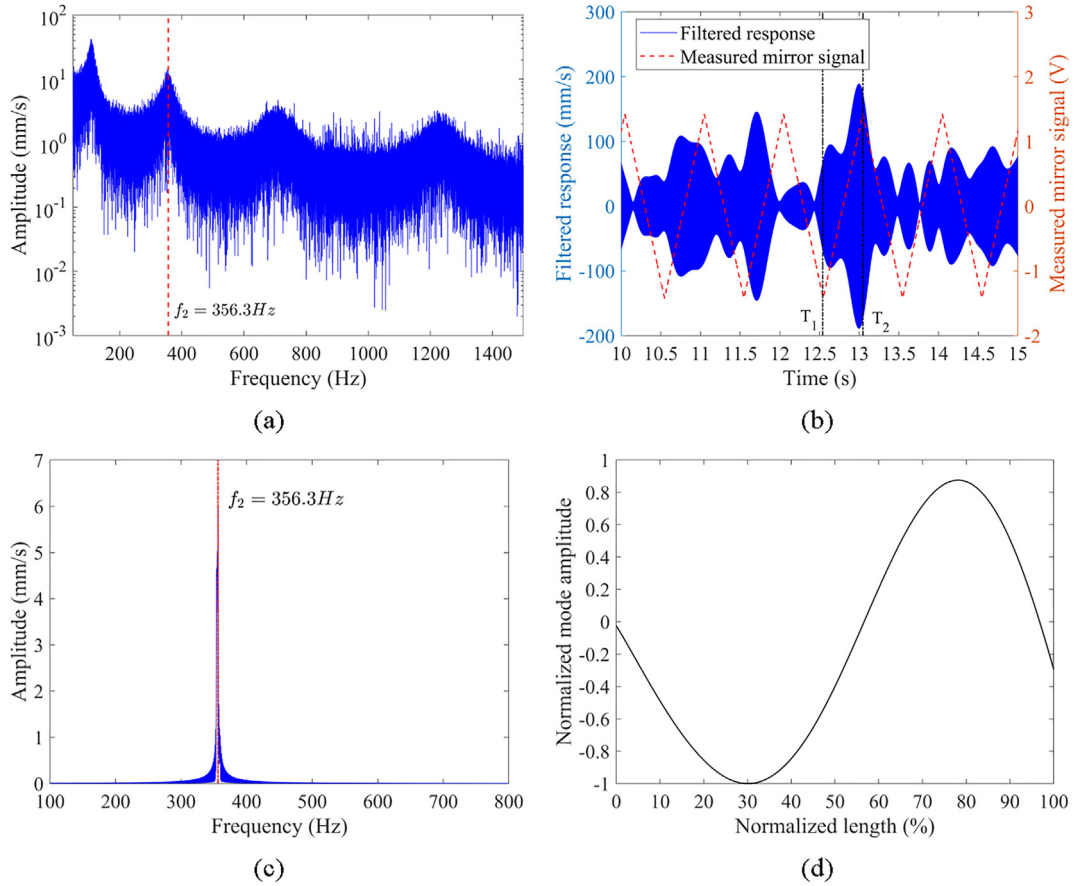
Fig. 6. (a) FFT of raw response of the beam under white-noise excitation in 1D CSLDV measurement with f_{sc} = 1 Hz and f_{sa} = 125 kHz, (b) the filtered response by a bandpass filter with the passband [356, 357] to allow only the damped natural frequency identified in (a) to pass through it and a time interval $[T_1, T_2]$ that is selected to obtain an end-to-end response of the beam, (c) the FFT of the filtered response in (b), and (d) the second normalized undamped end-to-end mode shape of the beam estimated by the extended demodulation method.

Table 1
Test conditions and estimated modal parameters of the beam from 1D CSLDV measurements with the same scanning frequency of 1 Hz and different sampling frequencies of 125, 50, and 25 kHz, and those with 1D step-wise scanning measurement.

		Step scan	f_{sa} = 125 kHz	f_{sa} = 50 kHz	f_{sa} = 25 kHz
Numbers of measurement points		101	62,500	25,000	12,500
Test durations		776 s	50 s	50 s	50 s
1st mode	Damped natural frequencies	107.4 Hz	107.2 Hz	106.7 Hz	112.7 Hz
	Errors	/	−0.2%	−0.7%	4.9%
	MAC values	/	99%	99%	96%
2nd mode	Damped natural frequencies	357.0 Hz	356.3 Hz	362.2 Hz	369.3 Hz
	Errors	/	−0.2%	1.5%	3.4%
	MAC values	/	97%	96%	96%
3rd mode	Damped natural frequencies	707.0 Hz	710.0 Hz	720.1 Hz	741.2 Hz
	Errors	/	0.4%	1.8%	4.9%
	MAC values	/	95%	94%	77%
4th mode	Damped natural frequencies	1217.6 Hz	1223.7 Hz	1253.6 Hz	1252.1 Hz
	Errors	/	0.5%	3%	2.8%
	MAC values	/	95%	60%	61%

beam from 1D CSLDV measurements with various scanning and sampling frequencies, and corresponding damped mode shapes from 1D step-wise scanning measurement are shown in Figs. 7 and 8.

It can be seen from Table 1 and Fig. 7 that the first and second undamped end-to-end mode shapes of the beam from 1D CSLDV measurements with different sampling frequencies are similar to each other and all have high MAC values, which are larger than 96%, with respect to corresponding damped mode shapes from step-wise scanning measurement. The third and

Table 2

Testing conditions and estimated modal parameters of the beam from 1D CSLDV measurements with the same sampling frequency of 125 kHz and different scanning frequencies of 1 and 0.5 Hz, and those with 1D step-wise scanning measurement.

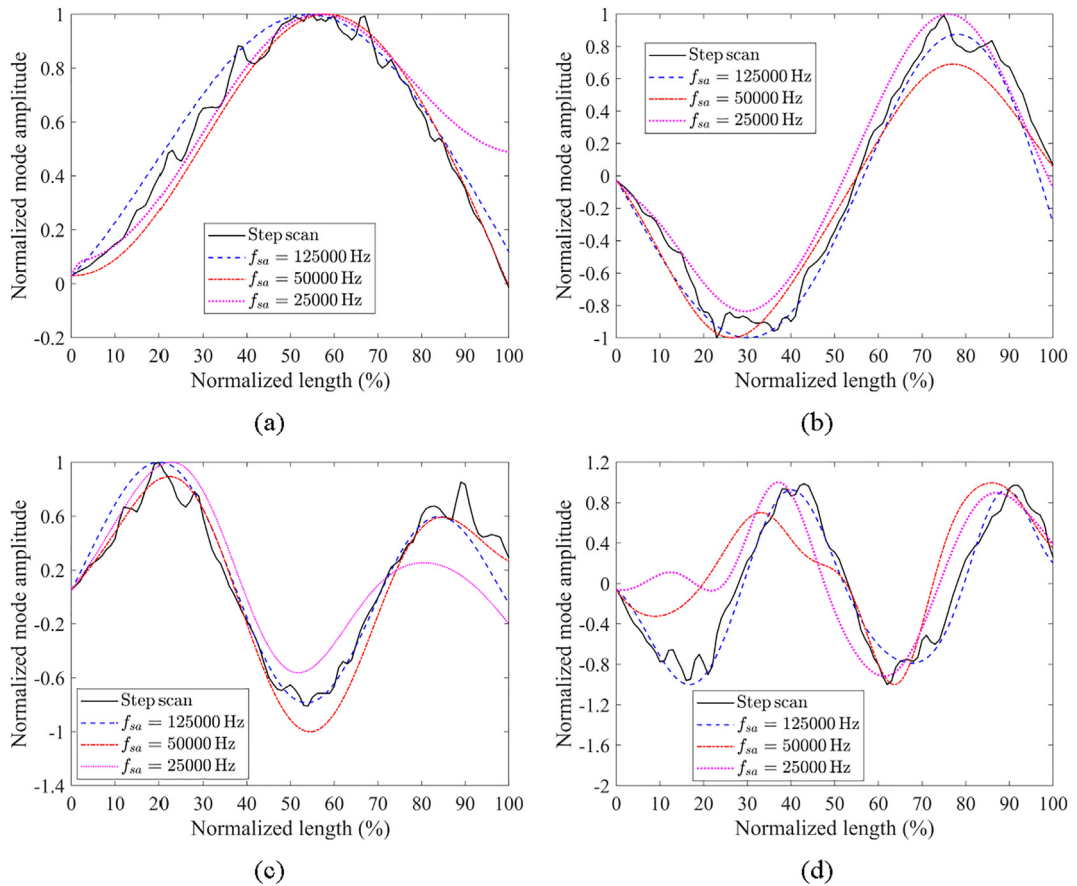|		Step scan	f_{sc} = 1 Hz	f_{sa} = 0.5 Hz
Number of measurement points		101	62,500	125,000
Test Durations		776 s	50 s	50 s
1st mode	Damped natural frequencies	107.4 Hz	107.2 Hz	108.1 Hz
	Errors	/	−0.2%	0.7%
	MAC values	/	99%	99.0%
2nd mode	Damped natural frequencies	357.0 Hz	356.3 Hz	352.2 Hz
	Errors	/	−0.2%	−1.3%
	MAC values	/	97%	97%
3rd mode	Damped natural frequencies	707.0 Hz	710.0 Hz	699.4 Hz
	Errors	/	0.4%	−1.1%
	MAC values	/	95%	95%
4th mode	Damped natural frequencies	1217.6 Hz	1223.7 Hz	1211.5 Hz
	Errors	/	0.5%	0.5%
	MAC values	/	95%	95%

Fig. 7. (a) First, (b) second, (c) third, and (d) fourth normalized 1D undamped end-to-end mode shapes of the beam from 1D CSLDV measurements with the same scanning frequency of 1 Hz and different sampling frequencies of 125, 50 and 25 kHz, and corresponding damped mode shapes from 1D step-wise scanning measurement.

fourth undamped mode shapes of the beam from 1D CSLDV measurements, however, are significantly affected by their sampling frequencies. Estimated third and fourth undamped mode shapes of the beam from 1D CSLDV measurements have high MAC values, which are about 95%, with respect to corresponding damped mode shapes from 1D step-wise scanning measurement when its sampling frequency is 125 kHz, but can have much lower MAC values for 1D CSLDV measurements with lower sampling frequencies. One can see that MAC values of the fourth undamped mode shapes of the beam from 1D CSLDV measurements with sampling frequencies of 50 and 25 kHz are close to 60%, which may not be acceptable in mode shape
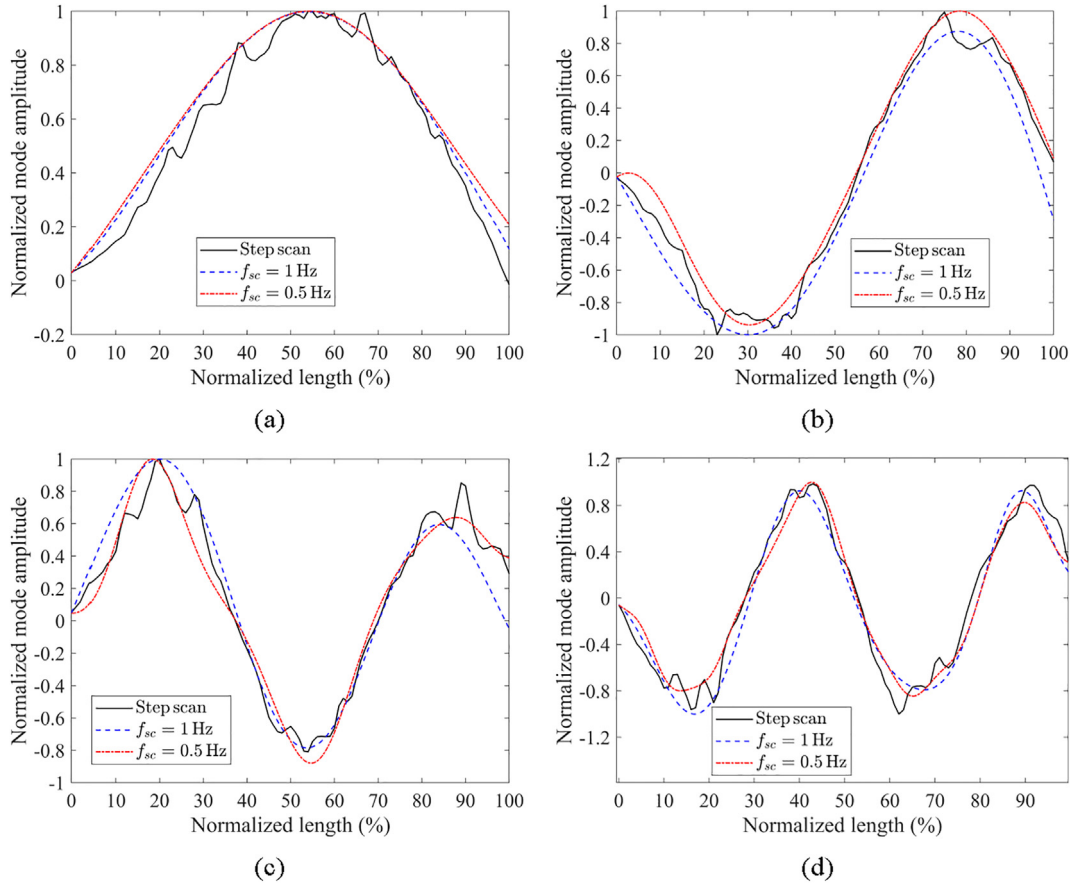
Fig. 8. (a) First, (b) second, (c) third, and (d) fourth normalized 1D undamped end-to-end mode shapes of the beam from 1D CSLDV measurements with the same sampling frequency of 125 kHz and different scanning frequencies of 1 and 0.5 Hz, and corresponding damped mode shapes from 1D step-wise scanning measurement.

estimation. Checking the fourth damped natural frequencies of the beam from 1D CSLDV measurements with sampling frequencies of 50 and 25 kHz in Table 1, one can find that errors between the fourth damped natural frequencies from 1D CSLDV measurements with above sampling frequencies and that from 1D step-wise scanning measurement are about 3%, which are much larger than the error between the fourth damped natural frequency from 1D CSLDV measurement with a sampling frequency of 125 kHz and that from 1D step-wise scanning measurement, which is less than 0.5%. As mentioned in the previous discussion, identifying the i-th damped natural frequency of the beam under white-noise excitation is a significant step of estimating its i-th undamped mode shape by the extended demodulation method, since it is directly related to the passband of the bandpass filter used to filter raw response. A possible reason for large errors between the fourth damped natural frequencies from 1D CSLDV measurements with low sampling frequencies and that from 1D step-wise scanning measurement is that low sampling frequencies cannot provide enough resolution in the FFT algorithm when their test durations are the same as that for CSLDV measurement with the high sampling frequency.

One can see from Table 2 and Fig. 9 that the first four undamped end-to-end mode shapes from 1D CSLDV measurements with two different scan frequencies are similar to each other and all have high MAC values, which are larger than 95%, with respect to corresponding damped mode shapes from 1D step-wise scanning measurement. Damped natural frequencies of the beam identified by the FFT of its raw response for the two 1D CSLDV measurements are close to those from 1D step-wise scanning measurement with errors less than 1.3%, since the resolution of the FFT algorithm is not affected by the scanning frequency of 1D CSLDV measurement. Note that undamped mode shapes of the beam from 1D CSLDV measurements are smoother than corresponding damped mode shapes from 1D step-wise scanning measurement due to their dense measurement points.

3.3. Estimated damped natural frequencies and 3D undamped end-to-end mode shapes of the test beam from 3D CSLDV measurement

Vibration of the beam under white-noise excitation can be synchronously measured by three CSLDVs with three different VCSs in the 3D CSLDV system by following instructions in Section 3.1, and transformed to vibration components in x, y, and z
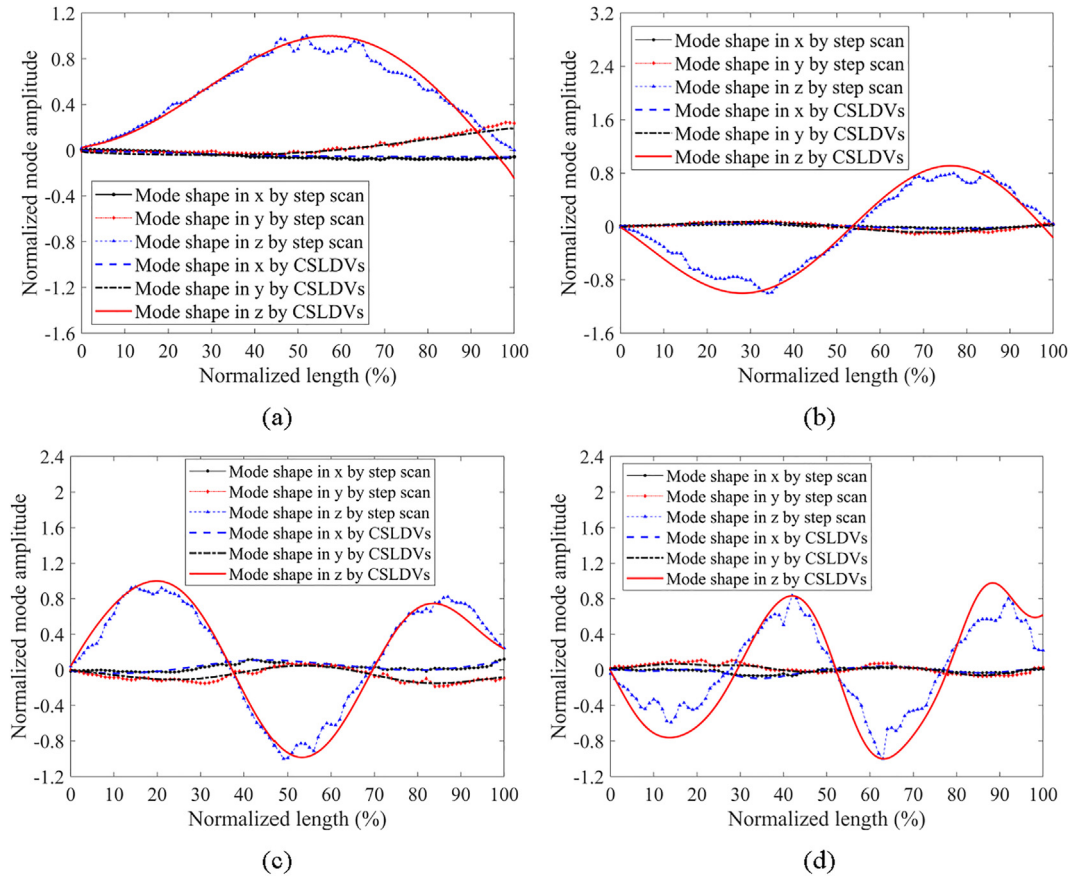
Fig. 9. (a) First, (b) second, (c) third, and (d) fourth normalized 3D undamped end-to-end mode shapes of the beam under white-noise excitation from 3D CSLDV measurement with a sampling frequency of 125 kHz and a scanning frequency of 1 Hz, and corresponding damped mode shapes from 3D step-wise scanning measurement.

directions of the same MCS in Fig. 4(b) using Eq. (12). The extended demodulation method proposed in this study can then be used to estimate 3D undamped end-to-end mode shapes of the beam in corresponding directions of the MCS. Similar to 1D vibration measurement in Section 3.2, 3D damped mode shapes of the beam from 3D step-wise scanning measurement are used as references to examine the accuracy of the 3D CSLDV system developed in this work. The first four normalized 3D undamped end-to-end mode shapes of the beam in x, y, and z directions, which are obtained from 3D CSLDV measurement with a sampling frequency of 125 kHz and a scanning frequency of 1 Hz, and its corresponding 3D damped mode shapes from 3D step-wise scanning measurement are shown in Fig. 9, and MAC values between them can be found in Table 3. Note that test conditions, including numbers of scan measurement points and test durations, of 3D CSLDV measurement and 3D step-wise scanning measurement are the same as those of 1D CSLDV measurement and 1D step-wise scanning measurement, respectively, since three laser spots synchronously move along the same scan line in a continuous manner and scan

Table 3
MAC values between the first four 3D undamped mode shapes of the beam under random excitation from 3D CSLDV measurement with a sampling frequency of 125 kHz and a scanning frequency of 1 Hz, and corresponding damped mode shapes from 3D step-wise scanning measurement.

Mode	MAC values		
	x direction	y direction	z direction
1st	97%	95%	99%
2nd	92%	95%	98%
3rd	90%	96%	97%
4th	92%	91%	94%

the same measurement point in a step-wise manner, respectively. Also, damped natural frequencies of the beam from the above 3D CSLDV measurement are the same as those from corresponding 1D CSLDV measurement, which can be found in Table 1 or 2. As mentioned in Section 3.1, the z direction in the MCS shown in Fig. 4(b) has the smallest angle with the excitation direction; so the vibration component of the beam in the z direction has the largest amplitude among those in three directions, and mode shapes shown in Fig. 9 are normalized by dividing their values by maximum absolute values of corresponding mode shape components in the z direction.

The first four 3D undamped end-to-end mode shapes of the beam obtained from the 3D CSLDV system all have high MAC values, which are larger than 94%, with respect to corresponding damped mode shapes from 3D step-wise scanning measurement in the z direction, and have slightly lower MAC values, which are larger than 90%, in x and y directions, as shown in Table 3. A possible reason for slightly lower MAC values of mode shape components in x and y directions is that vibration components in these two directions have much smaller amplitudes than that in the z direction and their SNRs are lower than that in the z direction for both CSLDV measurement and step-wise scanning measurement. It is concluded that the 3D CSLDV system has essentially the same level of accuracy as that of 3D step-wise scanning measurement in obtaining 3D mode shapes of the beam under white-noise excitation, but can measure much more points in much less time. Note that calibration in the 3D step-wise scanning manner is based on the image processing technique provided by the Polytec PSV-500 software, but calibration of the 3D CSLDV system developed in this work is based on visual observation as described in Section 3.1; so some more time can be taken in calibration of the 3D CSLDV system and slight errors may be introduced into final results.

4. Conclusions

A novel 3D CSLDV system, which contains three CSLDVs and an external controller, is developed in this work to measure 3D vibration of a structure under random excitation, and a new OMA method is proposed to estimate its 3D modal parameters, including damped natural frequencies and undamped end-to-end mode shapes, by extending the conventional demodulation method. Experimental investigation on 1D and 3D CSLDV measurements for natural frequency and mode shape estimation was conducted on a beam under white-noise excitation to validate the extended demodulation method and examine the accuracy of the 3D CSLDV system. Main conclusions from this work are shown below:

(1) With calibration among three CSLDVs in the 3D CSLDV system, rotational angles of its scan mirrors can be adjusted to ensure that three laser spots continuously and synchronously move along the same scan line on the beam.
(2) Errors between the first four damped natural frequencies of the beam under white-noise excitation from 1D CSLDV measurement with a sampling frequency of 125 kHz and those from 1D step-wise scanning measurement are less than 0.5%, and MAC values between the first four undamped mode shapes from the above CSLDV measurement and corresponding damped mode shapes from step-wise scanning measurement are larger than 95%, while errors between the fourth damped natural frequencies from CSLDV measurements and those from step-wise scanning measurement are about 3% when their sampling frequencies are 50 and 25 kHz, and corresponding MAC values are about 60%, indicating that high modal parameters of the beam estimated by the extended demodulation method can be significantly affected by sampling frequencies of CSLDV measurements since low sampling frequencies cannot provide enough resolution in the FFT algorithm to obtain accurate damped natural frequencies and an effective passband of the bandpass filter used in the extended demodulation method.
(3) Errors between the first four damped natural frequencies of the beam under white-noise excitation from 1D CSLDV measurements with scanning frequencies of 1 and 0.5 Hz and those from step-wise scanning measurement are less than 1.3%, and MAC values between the first four undamped mode shapes from above two CSLDV measurements and corresponding damped mode shapes from step-wise scanning measurement are larger than 95%, indicating that modal parameters of the beam estimated by the extended demodulation method are not affected by scanning frequencies of CSLDV measurements since the resolution of the FFT algorithm is not affected by the scanning frequency.
(4) MAC values between the first four undamped mode shapes of the beam under white-noise excitation from 3D CSLDV measurement and corresponding damped mode shapes from 3D step-wise scanning measurement are larger than 94% in the z direction of the specified MCS that has the smallest angle with the excitation direction, and corresponding MAC values are larger 90% in x and y directions of the MCS due to relatively low SNRs of vibration components in above two directions.
(5) The extended demodulation method used with the 3D CSLDV system has essentially the same level of accuracy as that of 3D step-wise scanning measurement in obtaining 3D vibration of a structure under random excitation and estimating its 3D modal parameters, but the 3D CSLDV system can scan much more measurement points in much less time and provide smoother mode shapes than those from 3D step-wise scanning measurement.

CRediT authorship contribution statement

K. Yuan: Methodology, Software, Validation, Writing - original draft. **W.D. Zhu:** Conceptualization, Methodology, Validation, Supervision, Funding acquisition, Writing - review & editing.

Declaration of Competing Interest

References

[1] S.J. Rothberg, Laser vibrometry: pseudo-vibrations, J. Sound Vib. 135 (1989) 516–522.

[2] S.J. Rothberg, M.S. Allen, P. Castellini, D. Di Maio, J.J.J. Dirckx, D.J. Ewins, B.J. Halkon, P. Muyshondt, N. Paone, T. Ryan, H. Steger, An international review of laser Doppler vibrometry: Making light work of vibration measurement, Opt. Lasers Eng. 99 (2017) 11–22.

[3] P. Sriram, J.I. Craig, S. Hanagud, A scanning laser Doppler vibrometer for modal testing,, Int. J. Anal. Exp. Modal Anal. 5 (1990) 155–167.

[4] B.J. Halkon, S.R. Frizzel, S.J. Rothberg, Vibration measurements using continuous scanning laser vibrometry: velocity sensitivity model experimental validation, Meas. Sci. Technol. 14 (6) (2003) 773–783.

[5] B.J. Halkon, S. Rothberg, Vibration measurements using continuous scanning laser vibrometry: advanced aspects in rotor applications, Mech. Syst. Sig. Process. 20 (6) (2006) 1286–1299.

[6] A.B. Stanbridge, D.J. Ewins, Modal testing using a scanning laser Doppler vibrometer, Mech. Syst. Sig. Process. 13 (2) (1999) 255–270.

[7] A.B. Stanbridge, D.J. Ewins, A.Z. Khan, Modal testing using impact excitation and a scanning LDV, Shock Vib. 7 (2) (2000) 91–100.

[8] M.S. Allen, M.W. Sracic, A new method for processing impact excited continuous-scan laser Doppler vibrometer measurements, Mech. Syst. Sig. Process. 24 (3) (2010) 721–735.

[9] S. Vanlanduit, P. Guillaume, J. Schoukens, Broadband vibration measurements using a continuously scanning laser vibrometer, Meas. Sci. Technol. 13 (10) (2002) 1574–1582.

[10] D. Di Maio, D.J. Ewins, Continuous Scan, a method for performing modal testing using meaningful measurement parameters Part I, Mech. Syst. Signal Process. 25 (8) (2011) 3027–3042.

[11] D.M. Chen, Y.F. Xu, W.D. Zhu, Damage identification of beams using a continuously scanning laser Doppler vibrometer system, J. Vib. Acoust. 138 (5) (2016) 051011.

[12] D.M. Chen, Y.F. Xu, W.D. Zhu, Experimental investigation of notch-type damage identification with a curvature-based method by using a continuously scanning laser Doppler vibrometer system, J. Nondestr. Eval. 36 (2) (2017) 38.

[13] D.M. Chen, Y.F. Xu, W.D. Zhu, Identification of damage in plates using full-field measurement with a continuously scanning laser Doppler vibrometer system, J. Sound Vib. 422 (2018) 542–567.

[14] Y.F. Xu, D.M. Chen, W.D. Zhu, Modal parameter estimation using free response measured by a continuously scanning laser Doppler vibrometer system with application to structural damage identification, J. Sound Vib. 485 (2020) 115536.

[15] S. Yang, M.S. Allen, Output-only modal analysis using continuous-scan laser Doppler vibrometry and application to a 20 kW wind turbine, Mech. Syst. Sig. Process. 31 (2012) 228–245.

[16] Y.F. Xu, D.M. Chen, W.D. Zhu, Operational modal analysis using lifted continuously scanning laser Doppler vibrometer measurements and its application to baseline-free structural damage identification, J. Vib. Control 25 (7) (2019) 1341–1364.

[17] W. Staszewski, B. Lee, R. Traynor, Fatigue crack detection in metallic structures with lamb waves and 3D laser vibrometry, Meas. Sci. Technol. 18 (3) (2007) 727.

[18] H. Weisbecker, B. Cazzolato, S. Wildy, S. Marburg, J. Codrington, A. Kotousov, Surface strain measurements using a 3D scanning laser vibrometer, Exp. Mech. 52 (7) (2012) 805–815.

[19] W. Xu, W.D. Zhu, S.A. Smith, M.S. Cao, Structural damage detection using slopes of longitudinal vibration shapes, J. Vib. Acoust. 138 (3) (2016) 034501.

[20] D.E. Montgomery, R.L. West, R.A. Burdisso, Acoustic radiation prediction of a compressor housing from three-dimensional experimental spatial dynamics modeling, Appl. Acoust. 47 (2) (1996) 165–185.

[21] P. O'Malley, T. Woods, J. Judge, J. Vignola, Five-axis scanning laser vibrometry for three-dimensional measurements of non-planar surfaces, Meas. Sci. Technol. 20 (11) (2009) 115901.

[22] D.M. Chen, W.D. Zhu, Investigation of three-dimensional vibration measurement by a single scanning laser Doppler vibrometer, J. Sound Vib. 387 (2017) 36–52.

[23] B. Weekes, D. Ewins, Multi-frequency, 3D ODS measurement by continuous scan laser Doppler vibrometry, Mech. Syst. Sig. Process. 58 (2015) 325–339.

[24] K.S. Arun, T.S. Huang, S.D. Blostein, Least-squares fitting of two 3-D point sets, IEEE Trans. Pattern Anal. Mach. Intell. 5 (1987) 698–700.

[25] C. Godfrey, A.W. Siddons, Modern Geometry, University Press, Cambridge, UK, 1912.

[26] L. Meirovitch, Analytical methods in vibrations, The Macmillan Co, 1967.

[27] T.K. Caughey, M.E.J. O'Kelly, Classical normal modes in damped linear dynamic systems, J. Appl. Mech. 32 (3) (1965) 583–588.

[28] D.J. Ewins, Modal Testing: Theory, Practice, and Application, second ed., Research Studies Press Ltd., Hertfordshire, UK, 2000.